Molecular basis for the ATPase-powered substrate translocation by the Lon AAA+ protease

Kaiming Zhang[a,1], Shanshan Li[a,1], Kan-Yen Hsieh[b], Shih-Chieh Su[b], Grigore D. Pintilie[a], Wah Chiu[a,c,2], and Chung-I Chang[b,d,2]

[a]Department of Bioengineering and James H. Clark Center, Stanford University, Stanford, CA 94305, USA

[b]Institute of Biological Chemistry, Academia Sinica, Taipei 11529, Taiwan

[c]CryoEM and Bioimaging Division, Stanford Synchrotron Radiation Lightsource, SLAC National Accelerator Laboratory, Stanford University, Menlo Park, CA 94025, USA

[d]Institute of Biochemical Sciences, College of Life Science, National Taiwan University, Taipei 10617, Taiwan

[1]These authors contributed equally to this work.

[2]To whom correspondence may be addressed. Email: wahc@stanford.edu or chungi@gate.sinica.edu.tw.

Abstract

The Lon AAA+ (adenosine triphosphatases associated with diverse cellular activities) protease (LonA) converts ATP-fuelled conformational changes into sufficient mechanical force to drive translocation of the substrate into a hexameric proteolytic chamber. To understand the structural basis for the substrate translocation process, we have determined the cryo-electron microscopy (cryo-EM) structure of *Meiothermus taiwanensis* LonA (MtaLonA) at 3.6 Å resolution in a substrate-engaged state. Substrate interactions are mediated by the dual pore-loops of the ATPase domains, organized in spiral staircase arrangement from four consecutive protomers in different ATP-binding and hydrolysis states; a closed AAA+ ring is nevertheless maintained by two disengaged ADP-bound protomers transiting between the lowest and highest position. The structure reveals a processive rotary translocation mechanism mediated by LonA-specific nucleotide-dependent allosteric coordination among the ATPase domains, which is induced by substrate binding.

Introduction

The Lon AAA+ protease (LonA) is an ATP-dependent protease conserved in prokaryotes and eukaryotic organelles. LonA assembles as a homohexamer with each protomer containing an N-terminal domain, a middle ATPase domain, and a C-terminal protease domain (Rotanova et al. 2006). In addition to LonA, other Lon-like proteases (LonB and LonC) with distinct ATPase domains have been characterized in thermophilic archaeal and bacterial species (Liao et al. 2012; Rotanova et al. 2004). LonA plays a major role in cellular protein homeostasis by degrading damaged or misfolded abnormal proteins, which prevents these unwanted protein species from forming toxic aggregates. LonA is also involved in the regulation of many biological processes by degrading specific regulatory proteins (Gur 2013). Similar to the fused AAA+ and protease domain organization of Lon, the membrane-anchored AAA+ proteases FtsH and related i/m-AAA proteases are specialized in membrane protein quality control although their ATPase domains belong to different clades of the AAA+ superfamily and the protease domains are non-homologs (Puchades et al. 2020; Sauer and Baker 2011).

Previous results have revealed many functional and structural features of LonA. The protease activity of LonA is dependent on the presence of Mg^{2+}, which binds to the protease

domain and induces the formation of open active-site structure (Su et al. 2016). The Lon protease domain with an open active-site conformation adopts a 6-fold symmetric hexameric ring (Botos et al. 2004; Cha et al. 2010; Liao et al. 2013; Su et al. 2016). By contrast, LonA with an inactive proteolytic active-site conformation exhibits an open-spiral hexameric structure (Botos et al. 2019; Duman and Löwe 2010). Therefore, the protease domain plays an important role in the closed-ring assembly of LonA. While ATP is required for LonA to degrade protein substrates efficiently, ADP is known to inhibit the protease activity of Lon. The crystal structure of the ADP-bound LonA hexamer has revealed how ADP may inhibit LonA activity by inducing the formation of a closed degradation chamber (Lin et al. 2016). A substrate-translocation model was posited based on the ADP-bound structure by assuming a structural transition between the nucleotide-free and ADP-bound states from two pairs of three non-neighboring protomers (Lin et al. 2016). However, the simple one-step transition model is not supported by recent cryo-EM structures of substrate-bound AAA+ proteins with the ATPase domains organized in spiral staircase arrangement around a centrally positioned substrate polypeptide chain (Monroe et al. 2017; Yu et al. 2018; de la Peña et al. 2018; Ripstein et al. 2017; Ho et al. 2018; Gates et al. 2017; White et al. 2018; Han et al. 2017; Ripstein et al. 2020).

Here, we report cryo-EM structures of *Meiothermus taiwanensis* LonA (MtaLonA) in a substrate-engaged state, determined at 3.6 Å resolution. Structural analysis suggests that both the substrate and ATP play an important role to induce a spiral staircase arrangement of the ATPase domains. Moreover, the structure reveals how binding of ATP and hydrolysis of ATP to ADP induce distinct nucleotide-induced conformational states in the six ATPase domains to enable a processive rotary translocation mechanism by LonA-specific allosteric coordination.

Results

Specimen preparation of LonA with a protein substrate

To capture MtaLonA in the substrate-engaged state, we assessed the degradation of Ig2 (25 kDa), a model substrate used previously (Su et al. 2016), by wild-type MtaLonA using the slowly hydrolyzable ATP analog, ATP-γ-S. At the optimal reaction temperature (55°C), MtaLonA is able to degrade Ig2 with ATP-γ-S, albeit much slower compared to ATP (**Figure 1—figure supplement 1**). The result suggests that Ig2 is productively translocated by MtaLonA utilizing ATP-γ-S. Therefore, for cryo-EM imaging, we purified MtaLonA in complex with Ig2, ATP-γ-S,

and bortezomib, which inhibits Lon protease activity by covalently binding to the catalytic serine in the protease domain, in order to trap MtaLonA in the process of translocating Ig2 without undergoing subsequent substrate proteolysis (Liao et al. 2013; Su et al. 2016)(See Methods for details).

Cryo-EM structure of LonA engaged in translocating substrate

The structure of the MtaLonA-Ig2-bortezomib-ATP-γ-S complex was determined to 3.6-Å resolution by cryo-EM (**Figure 1A, Figure 1—figure supplement 2, supplemental Table 1 and supplemental Video 1**). The six protease domains associate into a closed-ring structure with C6 symmetry (**Figure 1B**). The six ATPase domains also form a closed ring (**Figure 1B**). However, those from four consecutive protomers P1-P4 (designated in the PDB coordinate file as chains A-D) organize into a spiral staircase arrangement, with protomers P1 and P4 occupying the highest and the lowest positions, respectively (**Figure 1C**). These four protomers spiraling around an extended 11-residue polypeptide chain, likely representing a segment of unfolded substrate Ig2, of which the backbone is well resolved in the map. By contrast, the two relatively mobile promoters P5 and P6 (corresponding to chains E and F, respectively, in the PDB file) make no substrate contacts (**Figure 1D**). Notably, these disengaged protomers, referred previously to as "seam" protomers, break the spiral arrangement by making a loose association with each other, and with protomers P4 and P1, respectively, thereby maintaining a closed AAA+ ring (**Figure 1A and 1D**). Although the full-length construct of wild-type MtaLonA includes the N-terminal regions (residues 1-243) critical for substrate interaction, no density was found for these regions in our structures, likely due to their flexible nature.

The sequence of Ig2 and the polarity of the bound polypeptide chain could not be determined from the density map. A strand of 11 alanine residues was modeled, with the C-terminus facing inside the chamber because Lon is known to recognize exposed C-terminal degron from model substrates and kinetics study indicates that the order of substrate scissile-site delivery occurs from the C- to N-terminal direction (Mikita et al. 2013; Gur and Sauer 2008). Contacts to the substrate polypeptide chain are made by protomers P1-P4, mediated by residue Tyr397 from pore-loop 1 and residue Trp431 from pore-loop 2; both have been shown to be required for degrading Ig2 (Lin et al. 2016). The four pore-loop-1 Tyr397 residues contact Ig2 in a right-handed spiral arrangement, with amino acid residues i, i+2, i+4, and i+6 of the substrate

(**Figure 1D, supplemental Video 1**). Contrary to the well-resolved pore loops of substrate-engaged protomers P1-P4, those of the seam protomers P5 and P6 do not make contact with the substrate and are less well-resolved in the map (**Figure 1A and 1D**).

ATPase sites around the substrate-engaged AAA+ ring

To understand how the staircase arrangement of the pore-loops 1 and 2 engaging the substrate correlates with nucleotide binding and hydrolysis states in the protomers, we analyzed the cryo-EM map of the ATPase site located in between the large AAA-α/β and the small AAA-α domains. The resolution of the map is sufficient to identify the bound nucleotides in the ATPase sites in protomers P1-P4 (**Figure 2—supplement 1, Figure 2—supplement 2, and supplemental Video 1**). In protomer P1, the ATPase pocket is well ordered, with a bound ATP-γ-S, whose γ-phosphate interacts with the arginine finger (Arg finger) Arg484 from the clockwise neighboring protomer P2; the α- and β-phosphates are contacted by the sensor II, Arg541, in the cis protomer (**Figure 2A**). Similarly, in protomers P2 and P3, ATP-γ-S is found in the ATPase pocket with well-resolved density, with the γ-phosphate also contacted by the Arg finger. However, the sensor II Arg541 engages the β- and γ-phosphates of the bound ATP-γ-S in protomer P2 but solely with the γ-phosphate in protomer P3 (**Figure 2B and 2C**). As a result, the Arg finger and sensor II residues appear to present the scissile Pγ-Oβ bond of ATP-γ-S in the most suitable conformation for hydrolysis only in protomer P3. In contrast, the ATPase pocket of protomer P4, which occupies the lowest step of the substrate-bound staircase, is ADP-bound and more open than those of protomers P1-P3; the Arg finger from the protomer P5 is 15 Å away from the β-phosphate and the adjacent sensor II residue contacting α-phosphate is flexible (**Figure 2D**).

Interestingly, the AAA-α/β domain of the disengaged seam protomer P5 makes the least inter-protomer interaction and is highly mobile as indicated in the resolution map (**Figure 1—figure supplement 2E**) and Q score (**Figure 2—supplement 2**), which measures the local resolution (Kucukelbir et al. 2014) and structure resolvability (Pintilie et al.), respectively. The ATPase site has only broken density for the bound nucleotide and the Walker-A/B motifs (**Figure 2—supplement 1**); the Arg finger from protomer P6 and the sensor II are also unresolved. As mentioned above, the Arg finger R484 from protomer P5 is far from the bound

ADP in protomer P4; therefore, the protomer P5 ATPase site is likely bound to ADP also, but not ATP-γ-S.

The seam protomer P6 also has a mobile AAA-α/β domain. The resolution of the map at the ATPase pocket is nevertheless sufficient to reveal a bound ADP (**Figure 2—supplement 1**), probably due to its ordered neighboring protomer P1. The side chains of the Arg finger from protomer P1 and the sensor II residues, though located nearby, are not well resolved.

Substrate-induced allosteric coordination

In the substrate-engaged state, the spiral staircase arrangement of the AAA-α/β domains in the closed AAA+ ring, which is covalently fused to the closed protease ring, is made possible by several previously found LonA-specific structural features (Lin et al. 2016). They include nucleotide-dependent rigid-body rotation of the AAA-α/β domain, which presents the dual pore-loops, to adopt different positions with respect to the AAA-α domain. In addition, the flexible protease-domain (PD) linker bridging the AAA-α and the protease domains accommodate further rotational movement of the AAA-α domain (**Figure 3**).

Notably, the cis Arg finger Arg484 in the ATP-γ-S-bound protomers are positioned within the hydrogen-bonding distance near the bound nucleotide in the ATPase pocket of the counterclockwise neighboring protomer, making contact only with bound ATP-γ-S but not ADP (**Figure 2**). Interestingly, Arg484 is contacted by Asp444 and Pro445 in the N-terminal base-loop of the pre-sensor-1 β-hairpin (PS1βH), a motif conserved in LonA, HslU, and Clp AAA+ proteases (Iyer et al. 2004; Erzberger and Berger 2006). In the substrate-engaged, spirally arranged protomers P1-P3, the base-loop residues Asp444 and Glu446 form a trans-ATP-interacting group together with Arg484 to bind ATP-γ-S (**Figure 3—supplement 1**). Taken together, based on the structural results it is tempting to envisage that engaging the substrate polypeptide chain appears to induce the formation of a spiral staircase arrangement of ATP-bound protomers, enabling the interaction of the PS1βH base-loop and the Arg-finger with the ribose and the phosphate groups of ATP, respectively, and to facilitate ATP hydrolysis in the ATPase site. Our structure may thus offer a straightforward explanation of how the presence of protein or peptide substrates stimulates the ATPase activity of LonA, a hallmark feature also shared by other AAA+ proteases (Cheng et al. 2012; Goldberg et al. 1994; Seol et al. 1997; Waxman and Goldberg 1986; Yamada-Inagawa et al. 2003; Zhang and Wigley 2008).

Discussion

The main goal of the present work is to address the molecular basis for substrate translocation by LonA. Our cryo-EM structure of Ig2-bound wild-type MtaLonA suggest a LonA-specific processive rotary mechanism. An exposed substrate polypeptide chain containing the degron may be engaged by at least two flexible adjoining AAA-α/β domains via their pore-loops I. If the substrate-engaging protomer at the farthest counterclockwise position is ADP bound, its substrate-engaged and ATP-bound AAA-α/β domain may further stabilize the counterclockwise neighboring protomer in ATP-bound conformation; such allosteric inter-protomer interaction may propagate until a spiral staircase arrangement of four substrate-engaged protomers is reached, with bound ATP in the ATPase site between each "step" (**Figure 4**). As shown in our schematic model, after ATP hydrolysis proceeds to the next counterclockwise ATPase site, the ADP-bound protomer at the lowest step is disengaged from the substrate, becoming one of the two mobile seam protomers, until it is recruited by an ATP-bound protomer, which is capable of presenting the Arg finger and the PS1βH base-loop, to promote nucleotide exchange and binding with ATP. Of note, in coordinating the process of translocating substrate, every individual protomer traverses multiple cycles of four substrate-gripping conformers in the nucleotide-binding states ranging from ATP-bound to post-hydrolysis ADP-Pi states, plus two disengaged ADP-bound seam states, in sequential order.

The above mechanism featuring "hand-over-hand" substrate translocation coupled to counterclockwise sequential hydrolysis of ATP is therefore conserved in a variety of different AAA+ proteins (Monroe et al. 2017; Yu et al. 2018; de la Peña et al. 2018; Ripstein et al. 2017; Ho et al. 2018; Gates et al. 2017; White et al. 2018; Han et al. 2017; Ripstein et al. 2020). During the preparation of this manuscript, a preprint reporting the structure of a substrate-bound Walker-B mutant of LonA from *Yersinia pestis* (YpeLonA) also suggested a similar mechanism (Shin et al.). However, these substrate-bound structures show several notable differences. Despite containing four ATP-bound protomers in the staircase arrangement, YpeLonA engaged the substrate via only the highest three spiraling pore-loop I residues; in addition, the structure did not show direct interaction of the substrate with pore-loop 2. By contrast, MtaLonA binds to the substrate through the pore-loops from all four staircase protomers, with the lowest protomer of the staircase bound to ADP; such nucleotide arrangement in the substrate-engaging protomers has also been observed in the structure of a DNA-engaged state of the CMG helicase (Eickhoff et

al. 2019). Interestingly, both of the two different nucleotide-binding states captured in the YpeLonA and MtaLonA structures are distinct from those in other substrate-engaged AAA+ proteases (de la Peña et al. 2018; Dong et al. 2019; Puchades et al. 2017, 2019; Ripstein et al. 2020). It is likely that, although operated by a common mechanism, an AAA+ protease such as LonA may respond to different substrates, carrying different degrons, by employing protomers arranged spirally with different numbers of staircase steps to grip the substrate and to traverse different nucleotide-binding states to coordinate ATP hydrolysis, thereby generating different translocating forces. In this regard, future works on the analysis of the structures of an AAA+ protein with a series of substrates with different folding or stable states, and/or with different predefined degrons, may yield further insights into the mechanism of action of these molecular machines.

Materials and methods

Protein expression and purification

Cells were grown in LB medium at 37°C until the optical density reached 0.6 to 0.8. Isopropyl β-d-thiogalactopyranoside (IPTG) to a final concentration of 1 mM was then added to the culture and incubated for another 4 h at 25°C for full-length MtaLonA and 37°C for the substrate Ig2 (Lin et al. 2016; Su et al. 2016). Cells were harvested by centrifugation and suspended in lysis buffer containing 50 mM Tris-HCl (pH 8.0) and 500 mM NaCl. Cell lysate was first ruptured by a French press (Avestin) and centrifuge at 35,000 g. Supernatant was collected for 2.5 h binding with Ni-nitrilotriacetic acid resins (Qiagen) at 4°C. Protein was further washed with a stepwise imidazole gradient and eluted with 250 mM imidazole. After that, Ig2 was treated with TEV protease overnight to remove the 6xHis tag. All proteins were dialyzed against different buffer components to remove imidazole. MtaLonA was dialyzed against buffer containing 20 mM Tris-HCl (pH 8.0), 100 mM NaCl and 2 mM DTT, while Ig2 was dialyzed against 25 mM Tris-HCl (pH 8.0), 150 mM NaCl and 2 mM β-mercaptoethanol. The untagged Ig2 was further purified by Ni-NTA and Superdex 200 (GE Healthcare) chromatography.

After purification, MtaLonA was first incubated with 10 mM $MgCl_2$ for 1 h and then incubated with 1 mM bortezomib, 5 mM adenosine 5′-[γ-thio]-triphosphate (ATP-γ-S) and Ig2 (in 5-fold molar excess) overnight. The MtaLonA-Ig2-bortezomib-ATP-γ-S complex was then loaded onto Superdex 200 (GE Healthcare) column pre-equilibrated with 20 mM Tris-HCl

(pH8.0), 100 mM NaCl, 10 mM $MgCl_2$ and 2 mM DTT to remove unbound compounds. The protein complex was treated with additional 1 mM of ATP-γ-S before cryo-sample preparation.

Cryo-EM data acquisition

The samples were diluted at a final concentration of around 0.15 mg/mL for the substrate-engaged MtaLonA. Three microliters of the sample was applied onto glow-discharged 200-mesh R1.2/1.3 Quantifoil grids. The grids were blotted for 4 s and rapidly cryocooled in liquid ethane using a Vitrobot Mark IV (Thermo Fisher Scientific) at 4°C and 100% humidity. The samples were screened using a Talos Arctica cryo-electron microscope (Thermo Fisher Scientific) operated at 200 kV. They were then imaged in a Titan Krios cryo-electron microscope (Thermo Fisher Scientific) with GIF energy filter (Gatan) at a magnification of 215,000× (corresponding to a calibrated sampling of 0.65 Å per pixel) for the substrate-engaged state. Micrographs were recorded by EPU software (Thermo Fisher Scientific) with a Gatan K2 Summit direct electron detector, where each image was composed of 30 individual frames with an exposure time of 6 s and an exposure rate of 8.5 electrons per second per $Å^2$. A total of 1,800 movie stacks were collected.

Single-particle image processing and 3D reconstruction

All micrographs were first imported into Relion (Scheres 2012) for image processing. The motion-correction was performed using MotionCor2 (Zheng et al. 2017) and the contrast transfer function (CTF) was determined using CTFFIND4 (Rohou and Grigorieff 2015). All particles were autopicked using the NeuralNet option (threshold 1 = 0; threshold 2 = -5) in EMAN2 (Tang et al. 2007), and further checked manually. Then, particle coordinates were imported to Relion, where the poor 2D class averages were removed by several rounds of 2D classification. A total of 102,419 particles were transferred to cryoSPARC (Punjani et al. 2017) for ab-initio map generation. Then a good class with 58,276 particles was imported to Relion for 3D classification. After removing bad classes, the final 3D refinement was performed using 23,487 particles, and a 3.6 Å map was obtained.

Model building

The crystal structure of a hexameric LonA protease (PDB ID: 4YPL) from our previous work (Lin et al. 2016) was rigidly fitted into the cryo-EM map of substrate-engaged MtaLonA. As the six protomers were conformationally different in the cryo-EM density, molecular dynamics flexible fitting (MDFF) (Trabuco et al. 2008) was used. The MDFF was completed in three runs, where each run included 10^4 minimization steps and 10^5 molecular dynamics steps. After no noticeable deformation, the MDFF was stopped. The resultant models were refined using phenix.real_space_refine (Liebschner et al. 2019). The type of the bound nucleotide, ADP or ATP-γ-S, was determined by LigandFit in Phenix, with an overall correlation coefficient of the ligand to the map over 0.7. Then phenix.real_space_refine and Coot (Emsley et al. 2010) were applied for model optimization.

The final model was evaluated by MolProbity (Chen et al. 2010) and Q-scores (Pintilie et al.) as previously stated (Zhang et al. 2019). Statistics of the map reconstruction and model building are summarized in Table S1. The final structure model was analyzed with the PDBsum structure bioinformatics software (Laskowski et al. 2018) to identify key residues that interact with bound nucleotides. All figures were prepared using PyMol (Rigsby and Parker 2016) and Chimera (Pettersen et al. 2004).

Substrate degradation assay

Ig2 (domains 5 and 6 of the gelation factor ABP-120 of *Dictyostelium discoideum (Hsu et al. 2007)*) was used as the substrate in this assay. Then 4 mM of the substrate protein was incubated with 0.8 mM MtaLonA (hexamer) in the reaction buffer containing 50 mM Tri-HCl pH 8.0, 10 mM $MgCl_2$, 1 mM DTT, 5 mM ATP or ATP-γ-S at 55°C. At different time points, reaction aliquots were stopped by adding 5X SDS-PAGE loading dye and heated at 95°C for 5 min. The samples were then loaded onto a SurePAGE gel (4-20% Bis-Tris)(Genscript). Substrate protein bands were detected by Coomassie Blue staining.

Acknowledgments

We thank Kuei-Hsiang Pan and Lu-Chu Ke for their help on protein preparation. This work was supported by Academia Sinica and MOST grant 108-2320-B-001-011-MY3 (to C.I.C.) and the

National Institutes of Health grants (P41GM103832, R01GM079429, and S10OD021600 to W.C.).

Author contributions

C.-I.C. and W.C. conceived the study; C.I.C. and K.Z. designed experiments; K.Z. solved the structures; K.Z., S.L., and K.Y.H. performed experiments; K.Z., S.L., K.Y.H., G.D.P., W.C., and C.I.C. analyzed data; and K.Z., S.L., K.Y.H., W.C., and C.I.C. wrote the manuscript.

Data deposition

Cryo-EM map of the substrate-engaged MtaLonA with its associated atomic model have been deposited in the Electron Microscopy Data Bank and the Protein Data Bank under accession code EMD-21870, and PDB ID code 6WQH.

References

Botos I, Lountos GT, Wu W, Cherry S, Ghirlando R, Kudzhaev AM, Rotanova TV, de Val N, Tropea JE, Gustchina A, Wlodawer A. 2019. Cryo-EM structure of substrate-free E. coli Lon protease provides insights into the dynamics of Lon machinery. *Current Research in Structural Biology* **1**: 13–20. http://dx.doi.org/10.1016/j.crstbi.2019.10.001.

Botos I, Melnikov EE, Cherry S, Tropea JE, Khalatova AG, Rasulova F, Dauter Z, Maurizi MR, Rotanova TV, Wlodawer A, Gustchuhina A. 2004. The Catalytic Domain ofEscherichia coliLon Protease Has a Unique Fold and a Ser-Lys Dyad in the Active Site. *Journal of Biological Chemistry* **279**: 8140–8148. http://dx.doi.org/10.1074/jbc.m312243200.

Cha S-S, An YJ, Lee CR, Lee HS, Kim Y-G, Kim SJ, Kwon KK, De Donatis GM, Lee J-H, Maurizi MR, Kang SG. 2010. Crystal structure of Lon protease: molecular architecture of gated entry to a sequestered degradation chamber. *EMBO J* **29**: 3520–3530.

Cheng I, Mikita N, Fishovitz J, Frase H, Wintrode P, Lee I. 2012. Identification of a region in the N-terminus of Escherichia coli Lon that affects ATPase, substrate translocation and proteolytic activity. *J Mol Biol* **418**: 208–225.

Chen VB, Arendall WB 3rd, Headd JJ, Keedy DA, Immormino RM, Kapral GJ, Murray LW, Richardson JS, Richardson DC. 2010. MolProbity: all-atom structure validation for macromolecular crystallography. *Acta Crystallogr D Biol Crystallogr* **66**: 12–21.

de la Peña AH, Goodall EA, Gates SN, Lander GC, Martin A. 2018. Substrate-engaged 26 proteasome structures reveal mechanisms for ATP-hydrolysis-driven translocation. *Science* **362**. http://dx.doi.org/10.1126/science.aav0725.

329 Dong Y, Zhang S, Wu Z, Li X, Wang WL, Zhu Y, Stoilova-McPhie S, Lu Y, Finley D, Mao Y.
330 2019. Cryo-EM structures and dynamics of substrate-engaged human 26S proteasome.
331 *Nature* **565**: 49–55.

332 Duman RE, Löwe J. 2010. Crystal structures of Bacillus subtilis Lon protease. *J Mol Biol* **401**:
333 653–670.

334 Eickhoff P, Kose HB, Martino F, Petojevic T, Abid Ali F, Locke J, Tamberg N, Nans A, Berger
335 JM, Botchan MR, Yardimci H, Costa A. 2019. Molecular Basis for ATP-Hydrolysis-Driven
336 DNA Translocation by the CMG Helicase of the Eukaryotic Replisome. *Cell Rep* **28**: 2673–
337 2688.e8.

338 Emsley P, Lohkamp B, Scott WG, Cowtan K. 2010. Features and development of Coot. *Acta*
339 *Crystallogr D Biol Crystallogr* **66**: 486–501.

340 Erzberger JP, Berger JM. 2006. Evolutionary relationships and structural mechanisms of AAA+
341 proteins. *Annu Rev Biophys Biomol Struct* **35**: 93–114.

342 Gates SN, Yokom AL, Lin J, Jackrel ME, Rizo AN, Kendsersky NM, Buell CE, Sweeny EA,
343 Mack KL, Chuang E, Torrente MP, Su M, Shorter J, Southworth DR. 2017. Ratchet-like
344 polypeptide translocation mechanism of the AAA+ disaggregase Hsp104. *Science* **357**:
345 273–279.

346 Goldberg AL, Moerschell RP, Chung CH, Maurizi MR. 1994. ATP-dependent protease La (lon)
347 from Escherichia coli. *Methods Enzymol* **244**: 350–375.

348 Gur E. 2013. The Lon AAA+ protease. *Subcell Biochem* **66**: 35–51.

349 Gur E, Sauer RT. 2008. Recognition of misfolded proteins by Lon, a AAA protease. *Genes &*
350 *Development* **22**: 2267–2277. http://dx.doi.org/10.1101/gad.1670908.

351 Han H, Monroe N, Sundquist WI, Shen PS, Hill CP. 2017. The AAA ATPase Vps4 binds
352 ESCRT-III substrates through a repeating array of dipeptide-binding pockets. *Elife* **6**.
353 http://dx.doi.org/10.7554/eLife.31324.

354 Ho C-M, Beck JR, Lai M, Cui Y, Goldberg DE, Egea PF, Zhou ZH. 2018. Malaria parasite
355 translocon structure and mechanism of effector export. *Nature* **561**: 70–75.

356 Hsu S-TD, Fucini P, Cabrita LD, Launay H, Dobson CM, Christodoulou J. 2007. Structure and
357 dynamics of a ribosome-bound nascent chain by NMR spectroscopy. *Proc Natl Acad Sci U*
358 *S A* **104**: 16516–16521.

359 Iyer LM, Leipe DD, Koonin EV, Aravind L. 2004. Evolutionary history and higher order
360 classification of AAA+ ATPases. *J Struct Biol* **146**: 11–31.

361 Kucukelbir A, Sigworth FJ, Tagare HD. 2014. Quantifying the local resolution of cryo-EM
362 density maps. *Nat Methods* **11**: 63–65.

Laskowski RA, Jabłońska J, Pravda L, Vařeková RS, Thornton JM. 2018. PDBsum: Structural summaries of PDB entries. *Protein Sci* **27**: 129–134.

Liao J-H, Ihara K, Kuo C-I, Huang K-F, Wakatsuki S, Wu S-H, Chang C-I. 2013. Structures of an ATP-independent Lon-like protease and its complexes with covalent inhibitors. *Acta Crystallogr D Biol Crystallogr* **69**: 1395–1402.

Liao J-H, Kuo C-I, Huang Y-Y, Lin Y-C, Lin Y-C, Yang C-Y, Wu W-L, Chang W-H, Liaw Y-C, Lin L-H, Chang C-I, Wu S-H. 2012. A Lon-like protease with no ATP-powered unfolding activity. *PLoS One* **7**: e40226.

Liebschner D, Afonine PV, Baker ML, Bunkóczi G, Chen VB, Croll TI, Hintze B, Hung LW, Jain S, McCoy AJ, Moriarty NW, Oeffner RD, Poon BK, Prisant MG, Read RJ, Richardson JS,Richardson DC, Sammito MD, Sobolev OV, Stockwell DH, Terwilliger TC, Urzhumtsev AG, Videau LL, Williams CJ, Adams PD. 2019. Macromolecular structure determination using X-rays, neutrons and electrons: recent developments in Phenix. *Acta Crystallogr D Struct Biol* **75**: 861–877.

Lin C-C, Su S-C, Su M-Y, Liang P-H, Feng C-C, Wu S-H, Chang C-I. 2016. Structural Insights into the Allosteric Operation of the Lon AAA+ Protease. *Structure* **24**: 667–675.

Mikita N, Cheng I, Fishovitz J, Huang J, Lee I. 2013. Processive degradation of unstructured protein by Escherichia coli Lon occurs via the slow, sequential delivery of multiple scissile sites followed by rapid and synchronized peptide bond cleavage events. *Biochemistry* **52**: 5629–5644.

Monroe N, Han H, Shen PS, Sundquist WI, Hill CP. 2017. Structural basis of protein translocation by the Vps4-Vta1 AAA ATPase. *Elife* **6**. http://dx.doi.org/10.7554/eLife.24487.

Pettersen EF, Goddard TD, Huang CC, Couch GS, Greenblatt DM, Meng EC, Ferrin TE. 2004. UCSF Chimera--a visualization system for exploratory research and analysis. *J Comput Chem* **25**: 1605–1612.

Pintilie G, Zhang K, Su Z, Li S, Schmid MF, Chiu W. 2020. Measurement of Atom Resolvability in CryoEM Maps with Q-scores. *Nat Methods* **17**, 328–334. https://doi.org/10.1038/s41592-020-0731-1.

Puchades C, Ding B, Song A, Wiseman RL, Lander GC, Glynn SE. 2019. Unique Structural Features of the Mitochondrial AAA+ Protease AFG3L2 Reveal the Molecular Basis for Activity in Health and Disease. *Mol Cell* **75**: 1073–1085.e6.

Puchades C, Rampello AJ, Shin M, Giuliano CJ, Wiseman RL, Glynn SE, Lander GC. 2017. Structure of the mitochondrial inner membrane AAA+ protease YME1 gives insight into substrate processing. *Science* **358**. http://dx.doi.org/10.1126/science.aao0464.

Puchades C, Sandate CR, Lander GC. 2020. The molecular principles governing the activity and functional diversity of AAA+ proteins. *Nat Rev Mol Cell Biol* **21**: 43–58.

Punjani A, Rubinstein JL, Fleet DJ, Brubaker MA. 2017. cryoSPARC: algorithms for rapid unsupervised cryo-EM structure determination. *Nat Methods* **14**: 290–296.

Rigsby RE, Parker AB. 2016. Using the PyMOL application to reinforce visual understanding of protein structure. *Biochem Mol Biol Educ* **44**: 433–437.

Ripstein ZA, Huang R, Augustyniak R, Kay LE, Rubinstein JL. 2017. Structure of a AAA+ unfoldase in the process of unfolding substrate. *Elife* **6**. http://dx.doi.org/10.7554/eLife.25754.

Ripstein ZA, Vahidi S, Houry WA, Rubinstein JL, Kay LE. 2020. A processive rotary mechanism couples substrate unfolding and proteolysis in the ClpXP degradation machinery. *Elife* **9**. http://dx.doi.org/10.7554/eLife.52158.

Rohou A, Grigorieff N. 2015. CTFFIND4: Fast and accurate defocus estimation from electron micrographs. *J Struct Biol* **192**: 216–221.

Rotanova TV, Botos I, Melnikov EE, Rasulova F, Gustchina A, Maurizi MR, Wlodawer A. 2006. Slicing a protease: structural features of the ATP-dependent Lon proteases gleaned from investigations of isolated domains. *Protein Sci* **15**: 1815–1828.

Rotanova TV, Melnikov EE, Khalatova AG, Makhovskaya OV, Botos I, Wlodawer A, Gustchina A. 2004. Classification of ATP-dependent proteases Lon and comparison of the active sites of their proteolytic domains. *Eur J Biochem* **271**: 4865–4871.

Sauer RT, Baker TA. 2011. AAA+ proteases: ATP-fueled machines of protein destruction. *Annu Rev Biochem* **80**: 587–612.

Scheres SHW. 2012. RELION: implementation of a Bayesian approach to cryo-EM structure determination. *J Struct Biol* **180**: 519–530.

Seol JH, Yoo SJ, Shin DH, Shim YK, Kang MS, Goldberg AL, Chung CH. 1997. The heat-shock protein HslVU from Escherichia coli is a protein-activated ATPase as well as an ATP-dependent proteinase. *Eur J Biochem* **247**: 1143–1150.

Shin M, Asmita A, Puchades C, Adjei E, Luke Wiseman R, Wali Karzai A, Lander GC. 2019. Distinct Structural Features of the Lon Protease Drive Conserved Hand-over-Hand Substrate Translocation. http://dx.doi.org/10.1101/617159.

Su S-C, Lin C-C, Tai H-C, Chang M-Y, Ho M-R, Babu CS, Liao J-H, Wu S-H, Chang Y-C, Lim C, Chang C-I. 2016. Structural Basis for the Magnesium-Dependent Activation and Hexamerization of the Lon AAA+ Protease. *Structure* **24**: 676–686.

Tang G, Peng L, Baldwin PR, Mann DS, Jiang W, Rees I, Ludtke SJ. 2007. EMAN2: an extensible image processing suite for electron microscopy. *J Struct Biol* **157**: 38–46.

Trabuco LG, Villa E, Mitra K, Frank J, Schulten K. 2008. Flexible fitting of atomic structures into electron microscopy maps using molecular dynamics. *Structure* **16**: 673–683.

435 Vieux EF, Wohlever ML, Chen JZ, Sauer RT, Baker TA. 2013. Distinct quaternary structures of
436 the AAA+ Lon protease control substrate degradation. *Proc Natl Acad Sci U S A* **110**:
437 E2002–8.

438 Waxman L, Goldberg AL. 1986. Selectivity of intracellular proteolysis: protein substrates
439 activate the ATP-dependent protease (La). *Science* **232**: 500–503.

440 White KI, Zhao M, Choi UB, Pfuetzner RA, Brunger AT. 2018. Structural principles of SNARE
441 complex recognition by the AAA+ protein NSF. *Elife* **7**.
442 http://dx.doi.org/10.7554/eLife.38888.

443 Yamada-Inagawa T, Okuno T, Karata K, Yamanaka K, Ogura T. 2003. Conserved pore residues
444 in the AAA protease FtsH are important for proteolysis and its coupling to ATP hydrolysis.
445 *J Biol Chem* **278**: 50182–50187.

446 Yu H, Lupoli TJ, Kovach A, Meng X, Zhao G, Nathan CF, Li H. 2018. ATP hydrolysis-coupled
447 peptide translocation mechanism of Mycobacterium tuberculosis ClpB. *Proceedings of the*
448 *National Academy of Sciences* **115**: E9560–E9569.
449 http://dx.doi.org/10.1073/pnas.1810648115.

450 Zhang K, Li S, Kappel K, Pintilie G, Su Z, Mou T-C, Schmid MF, Das R, Chiu W. 2019. Cryo-
451 EM structure of a 40 kDa SAM-IV riboswitch RNA at 3.7 Å resolution. *Nat Commun* **10**:
452 5511.

453 Zhang X, Wigley DB. 2008. The "glutamate switch" provides a link between ATPase activity
454 and ligand binding in AAA+ proteins. *Nat Struct Mol Biol* **15**: 1223–1227.

455 Zheng SQ, Palovcak E, Armache J-P, Verba KA, Cheng Y, Agard DA. 2017. MotionCor2:
456 anisotropic correction of beam-induced motion for improved cryo-electron microscopy. *Nat*
457 *Methods* **14**: 331–332.

458

459

460

461

462

463

464

465

466

467

468

Figures

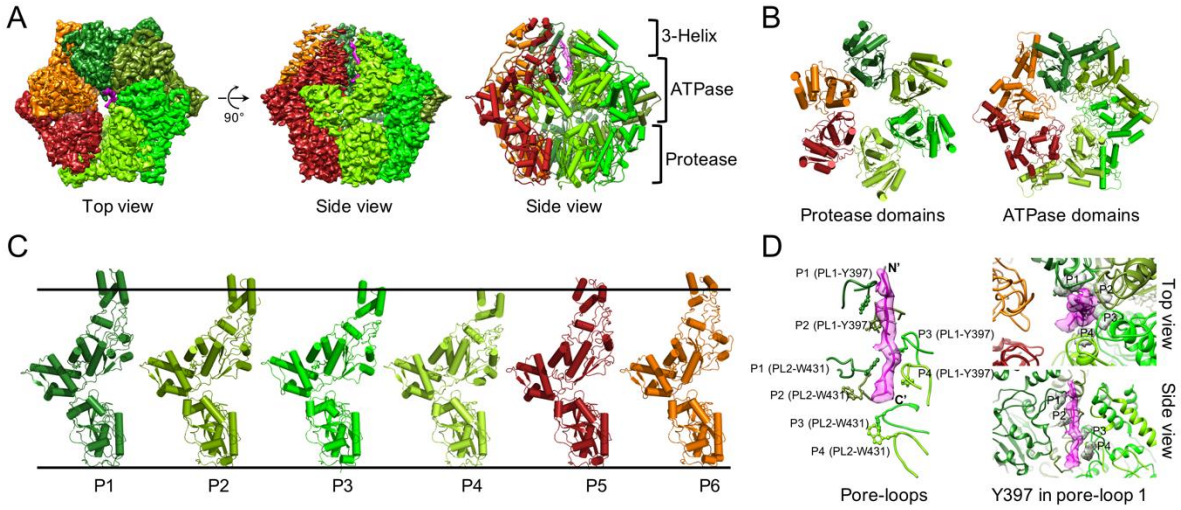

Figure 1. Overall structure of the substrate-bound MtaLonA complex. (**A**) The 3.6-Å cryo-EM map (left and middle) and model (right) of MtaLonA bound to the substrate Ig2 (magenta). The three structural domains are indicated on the right. (**B**) The rings of protease domains (res. 590-780; left) and ATPase domains (res. 307-583; right) in a top view. (**C**) Individual protomers (protomers P1-P6), which were aligned using the protease domain as the reference. (**D**) Pore-loop 1 (PL1) and 2 (PL2) residues from the protomers P1-P4 interacting with Ig2 (magenta density) are indicated. N' and C' denote N- and C-terminal ends, respectively.

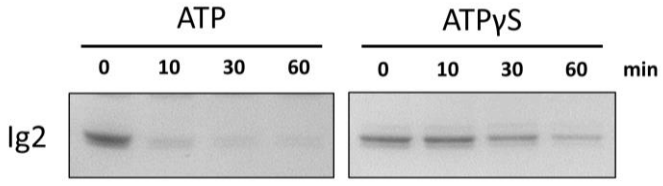

Figure 1—figure supplement 1. Substrate degradation assay. The substrate protein (Ig2) was degraded by wild-type MtaLonA in the presence of ATP (left) or ATP-γ-S (right).

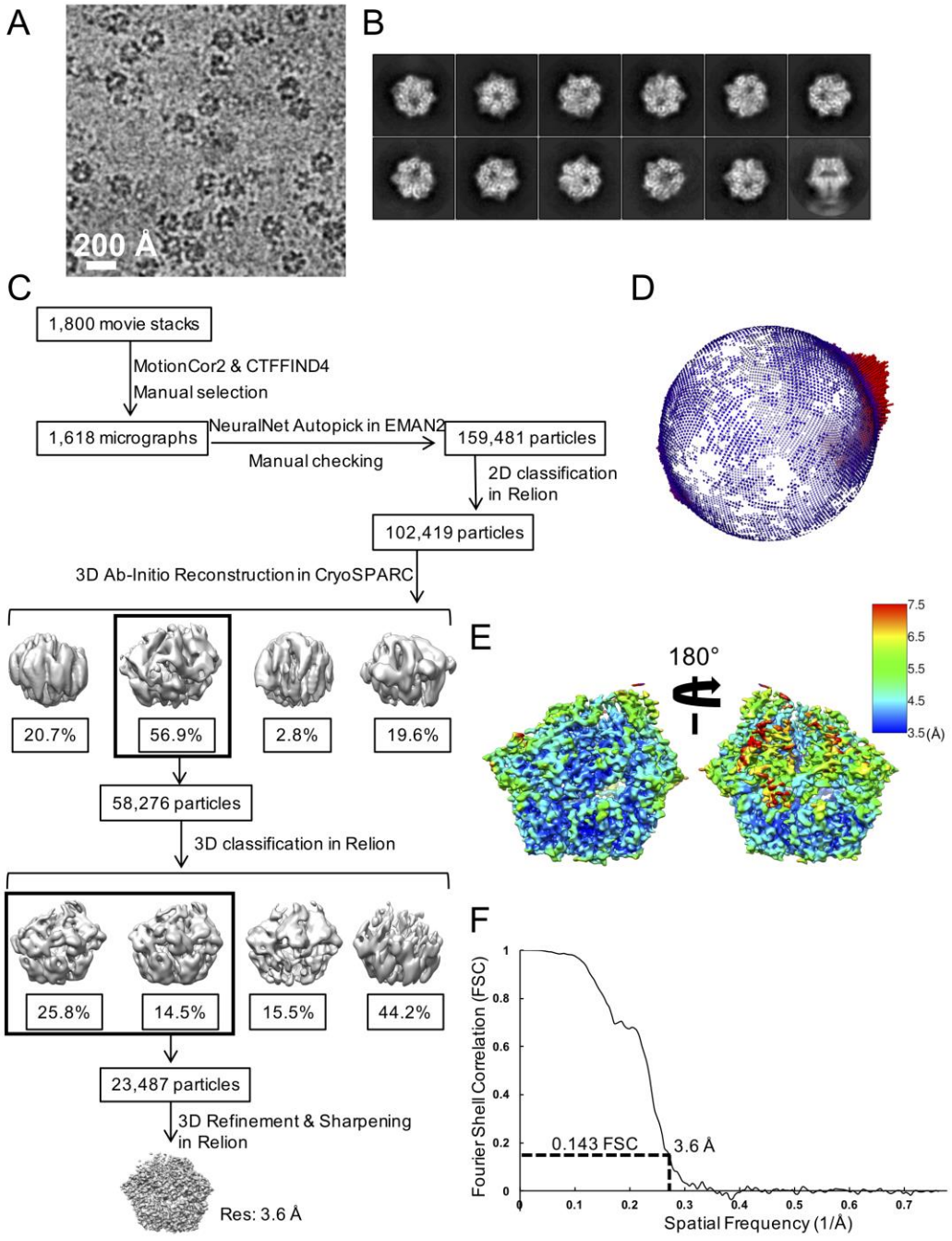

Figure 1—figure supplement 2. Single-particle cryo-EM analysis of the substrate-engaged MtaLonA. (**A**) Representative motion-corrected cryo-EM micrograph. (**B**) Reference-free 2D class averages. (**C**) Workflow of cryo-EM data processing. (**D**) Euler angle distribution of all particles used for calculating the final 3D reconstruction. (**E**) Resolution map for the final 3D reconstruction. (**F**) Gold standard FSC plot for the final 3D reconstruction.

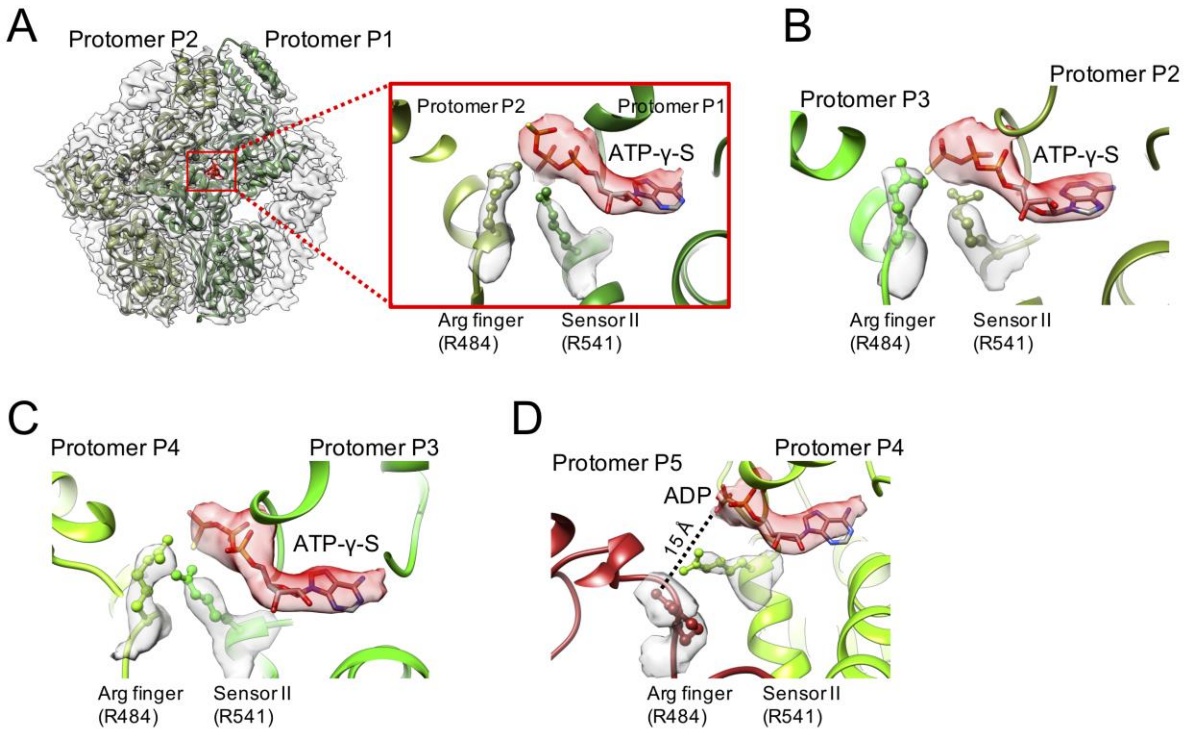

Figure 2. ATPase sites surrounding the substrate-engaged AAA+ ring. (**A**) The arginine finger and sensor II residues interacting with the ATP-γ-S bound to protomer P1. (**B**) The arginine finger and sensor II residues interacting with the ATP-γ-S bound to protomer P2. (**C**) The arginine finger and sensor II residues interacting with the ATP-γ-S bound to protomer P3. (**D**) The arginine finger and sensor II residues do not interact with ADP bound to protomer P4. The bound nucleotide is shown in red density with the fitted model.

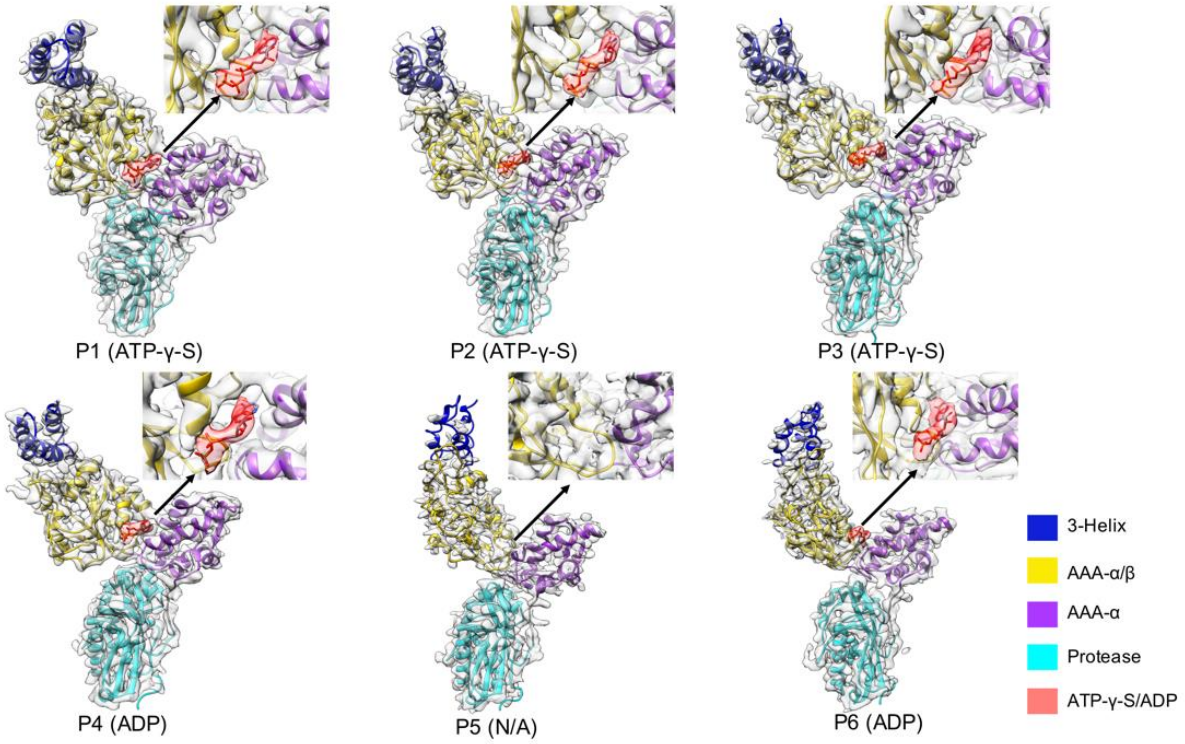

Figure 2—supplement 1. Identification of the bound nucleotide in the ATPase sites of protomers P1-P6. The nucleotide density with fitted model is shown in the insets. Different domains are shown in different colors.

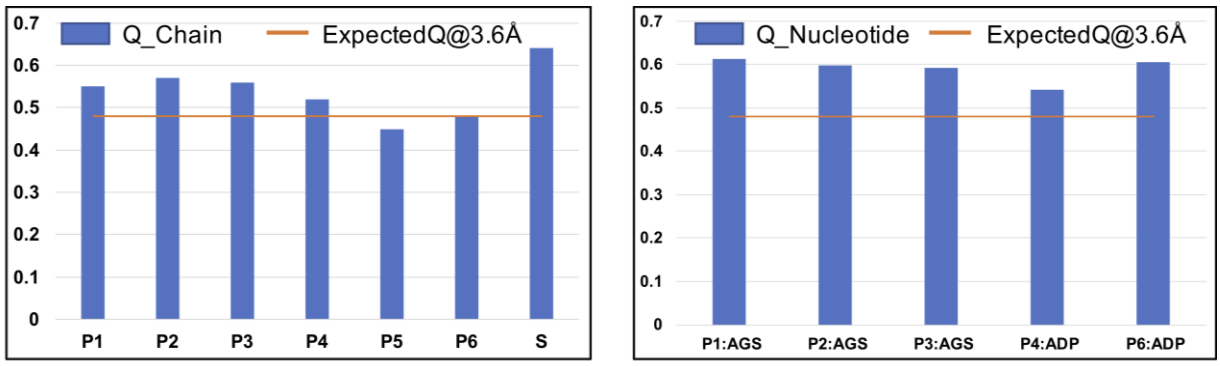

Figure 2—supplement 2. Resolvability of the cryo-EM structure of MtaLonA complexes calculated by Q-score. Q-score for each chain and nucleotide in model and map; the orange line represents the expected Q-score at respective resolution based on the correlation between Q-scores and map resolution of proteins. The higher Q-score indicates better resolvability. S refers to the substrate Ig2.

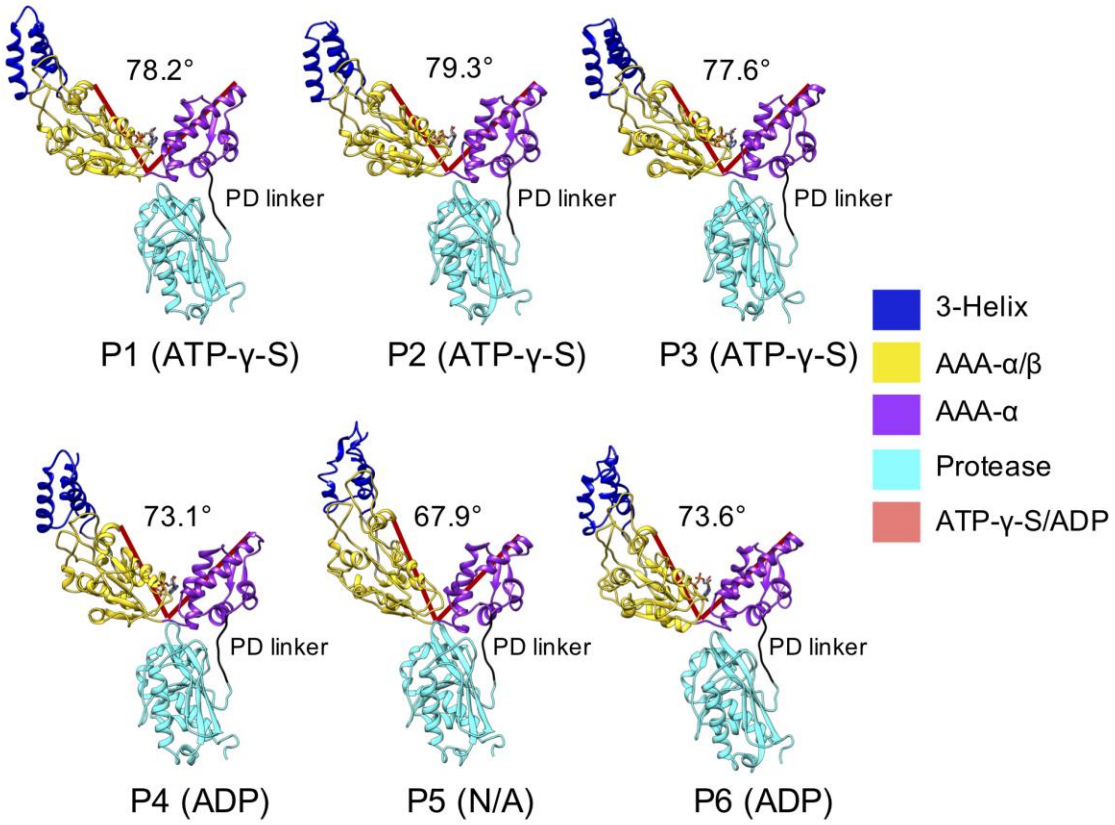

Figure 3. Nucleotide-dependent rigid-body rotation of the AAA-α/β domain. Individual protomers (protomers P1-P6) were aligned based on the AAA-α domain. The dihedral angles between the AAA-α/β and AAA-α domains are shown by using the Ca atom of Leu559, Gly492, and Gln411 as reference points for measurement of the angles. The protease-domain (PD) linker (res. 584-589) is shown in black.

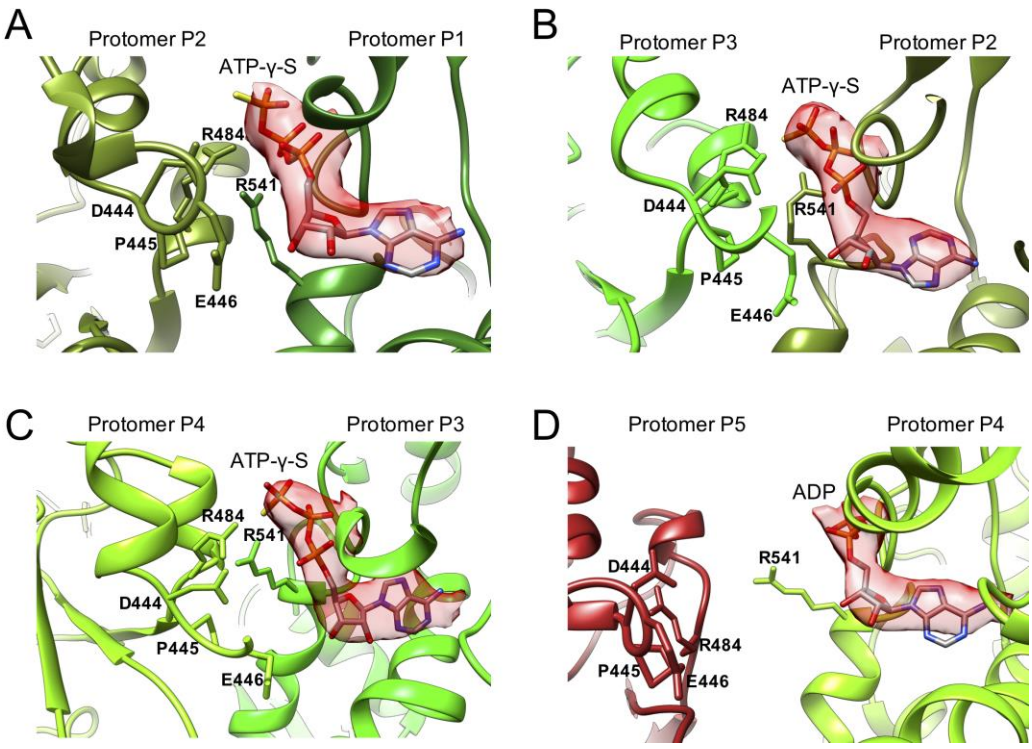

Figure 3—supplement 1. Conformation of the PS1βH base-loop (Asp444, Pro445, Glu446) and Arg-finger (Arg484) in the nucleotide-binding pocket between the neighboring protomers The bound nucleotide is shown in red density with the model fitted in.

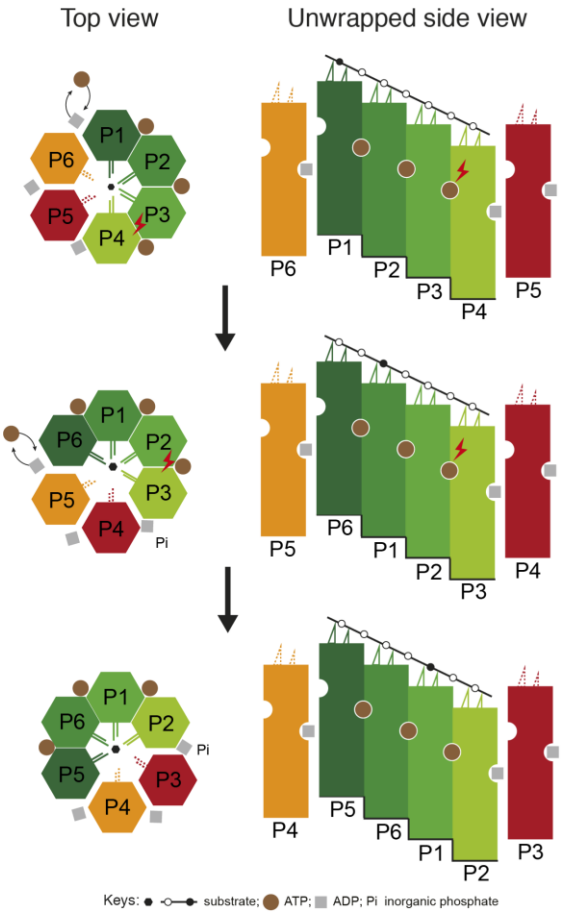

Figure 4. Structure-based model proposed for the processive substrate translocation by MtaLonA. Top-view (left) and unwrapped side-view (right) diagrams are illustrated to depict two sequential ATP hydrolysis events, which proceed counterclockwise, driving the movement of the substrate polypeptide chain, which is engaged by four protomers in four different conformational states, shown in different shades of green colors. The protomers are shown in the side view as long rectangles in a staircase arrangement, with the notches on the left and right sides representing the trans-ATP-interacting and the ATPase sites, respectively. The pore-loops 1 and 2 are depicted by double lines in the top view and long triangles in the side view. Dashed lines denote a flexible structure in the two disengaged protomer states (in brick red and orange colors). Proposed hydrolysis and nucleotide-exchange sites are depicted by lighting symbols and curved arrow pairs, respectively. Polypeptide chain in the side-view diagram is denoted by a straight line with open circles marking each of the amino acid residues. Translocation of the substrate is indicated by the shifting location of a specific amino acid represented by a closed circle.

Supplemental Table 1. Cryo-EM data collection, processing, and model validation

	Substrate-engaged MtaLonA
Data collection and processing	
Microscope	Titan Krios
Voltage (kV)	300
Camera	Gatan K2 Summit
Pixel size (Å)	0.65
Total Dose (e-/Å2)	51
Exposure time (s)	6
Number of frames per exposure	30
Defocus range (μm)	-0.6 - -2.6
Number of micrographs	1,800
Number of initial particles	159,481
Number of particles for 3D analyses	102,419
Symmetry	C1
Number of final particles	23,487
Resolution (0.143 FSC, Å)	3.6
Atomic model refinement	
Software	phenix.real_space_refine
Clash score	21.78
MolProbity score	2.32
Poor rotamers	0.51%
Favored rotamers	92.35%
Ramachandran outliers	0.22%
Ramachandran favored	91.81%
Bad bonds	0.03%
Bad angles	0.04%

546 **Supplemental Video 1.** The cryo-EM map of the substrate-bound MtaLonA complex with the
547 model fitted in. Four Tyr397 residues from the pore-loop 1 of protomers P1-P4 contact the
548 substrate (Ig2) in a right-handed spiral arrangement. The nucleotides in the ATPase domain in
549 protomers P6, P1, P2, P3, and P4 are shown in an amplified view sequentially.